Journal of Hazardous Materials 190 (2011) 381–390

Contents lists available at ScienceDirect

Journal of Hazardous Materials

journal homepage: www.elsevier.com/locate/jhazmat

Enhanced removal of Cr(VI) from aqueous solution using polypyrrole/Fe_3O_4 magnetic nanocomposite

Madhumita Bhaumik[a], Arjun Maity[b], V.V. Srinivasu[c], Maurice S. Onyango[a,*]

[a] Department of Chemical and Metallurgical Engineering, Tshwane University of Technology, Private Bag X680, Pretoria, South Africa
[b] Polymers and Composites, Council for Scientific and Industrial Research (CSIR), Pretoria, South Africa
[c] Department of Physics, University of South Africa (UNISA), Pretoria, South Africa

ARTICLE INFO

Article history:
Received 17 December 2010
Received in revised form 9 March 2011
Accepted 15 March 2011
Available online 24 March 2011

Keywords:
Magnetic nanocomposite
Polypyrrole
Adsorption
Hexavalent chromium
Equilibrium
Kinetics

ABSTRACT

Fe_3O_4 coated polypyrrole (PPy) magnetic nanocomposite was prepared via in situ polymerization of pyrrole monomer for the removal of highly toxic Cr(VI). Structure and morphology of the prepared nanocomposite were characterized by attenuated total reflectance Fourier transform infrared spectroscopy (ATR-FTIR), X-ray diffraction pattern, Field emission scanning electron microscopy (FE-SEM) and high resolution transmission electron microscopy (HR-TEM). Electron spin resonance (ESR) studies confirmed that the nanocomposite is magnetic in nature. Up to 100% adsorption was found with 200 mg/L Cr(VI) aqueous solution at pH 2. Adsorption of Cr(VI) on the surface of the adsorbent was confirmed by the ATR-FTIR and X-ray photoelectron spectroscopy (XPS). XPS studies also suggested that ion exchange and reduction on the surface of the nanocomposite may be the possible mechanism for Cr(VI) removal by the PPy/Fe_3O_4 nanocomposite. Adsorption results showed that Cr(VI) removal efficiency by the nanocomposite decreased with an increase in pH. Adsorption kinetics was best described by the pseudo-second-order rate model. Isotherm data fitted well to the Langmuir isotherm model. Thermodynamic study revealed that the adsorption process is endothermic and spontaneous in nature. Desorption experiment showed that in spite of the very poor recovery of the adsorbed Cr(VI); the regenerated adsorbent can be reused successfully for two successive adsorption–desorption cycles without appreciable loss of its original capacity.

1. Introduction

The presence of high concentration of heavy metals such as Cr, Hg, Cd, Ni, Co and Pb in both natural water supplies and industrial wastewater streams, is a critical health and environmental issue due to their high toxicity and bioaccumulation through the food chain and hence in the human body. Among these heavy metals Cr is considered as a major pollutant. Chromium and its compounds are extensively used in electroplating, leather tanning, metal finishing, nuclear power plant, dying, photography industries and textile industries [1,2]. In aqueous solution Cr exists both in trivalent (Cr(III)) and hexavalent (Cr(VI)) forms. Trivalent chromium is considered as an essential micronutrient for human, plant and animal metabolism and less toxic than Cr(VI) which is extremely mobile in the environment and very toxic, carcinogenic and mutagenic to living organism [3,4]. The US Environmental Protection Agency (EPA) recommended maximum allowable limit for Cr(VI) discharge into inland surface water is 0.1 mg/L and in portable water is 0.05 mg/L [5]. Effluents from certain industries often contain values higher than those and therefore, it is necessary to reduce the Cr(VI) concentration to acceptable level before discharging into the environment.

Several technologies have been employed to reduce/remove Cr(VI) from aqueous solutions such as chemical redox followed by precipitation, ion exchange, membrane process, electrodialysis and adsorption [6]. The major drawbacks associated with precipitations are: large consumption of reagents, high volume of sludge generation and inefficient recovery of treated metals for reuse [7]. Ion exchange, membrane processes and electrodialysis are not economically attractive because of their high operational costs [8]. Of these technologies, adsorption is a versatile and cost-effective technique for the removal of contaminants from water and hence has attracted attention in recent years [9].

Various adsorption media have been widely used for Cr(VI) removal. These include; activated carbon from different sources [10–12], biomaterials [13,14], metal oxides [15,16], hydrous metal oxides [17–19] and hybrid materials [20], among others. Recently, nanostructured materials have been used for Cr(VI) removal from water/wastewater and have proven advantageous over traditional adsorbents due to very large surface area, accessible active sites

* Corresponding author. Tel.: +27 123823533; fax: +27 123823532.
E-mail addresses: amaity@csir.co.za (A. Maity), OnyangoMS@tut.ac.za, onyi72uk@yahoo.co.uk (M.S. Onyango).

0304-3894/$ – see front matter © 2011 Elsevier B.V. All rights reserved.
doi:10.1016/j.jhazmat.2011.03.062

and a short diffusion length, which result in high adsorption capacity, rapid extraction dynamics and high adsorption efficiencies [21,22]. However, most of the nanomaterials have some limitations in adsorption and separation of pollutants from large volume of environmental samples. When column dynamic separation mode is used, the nanosized particle packed on column exhibit high back pressure and it is very difficult to achieve high flow rates and in case of static batch mode, nanosized adsorbents lead to a very low subsequent filtration rate [22]. Therefore, it is advantageous to develop a well dispersed nanoadsorbent with large surface area and suitable surface functionality that can remove Cr(VI) from large volume of environmental water.

The application of magnetic nanoparticles has attracted attention to solve environmental problems [7,23,24]. This is because magnetic nanoparticles besides having large surface area are highly dispersible in water and exhibit superparamagnetic properties. The latter property makes them separable from aqueous solution by the application of external magnetic field [25]. As such studies have explored application of different nanosized magnetic particles for the removal of Cr(VI) from water. Among the materials studied include; maghemite, magnetite (Fe_3O_4), diatomite supported/unsupported magnetite nanoparticles and surface modified jecobosite nanoparticles [7,26–28]. Most of these magnetic nanomaterials, however, have low capacities for Cr(VI) [7,26,27]. It is therefore imperative to develop new materials with improved capacity for Cr(VI).

In this study, iron oxide (Fe_3O_4) nanoparticles were encapsulated by polypyrrole (PPy) to achieve a well dispersed sorbent that can be magnetically separated and has a high capacity for Cr(VI). Polypyrrole has attracted much attention due to its unique properties of high electrical conductivity, relatively good environmental stability, nontoxicity, relatively low cost and ease of preparation which are favourable for various types of applications [29,30]. It was found that PPy carries charges via some of positively charged nitrogen atoms in the polymer matrix. To maintain charge neutrality, some of the counter ions are incorporated into the growing polymer chain [31]. The existence of positively charged nitrogen atoms in PPy provides a good prospect for its applications in adsorption or filtration separation [32,33]. Although PPy coated on wood sawdust has been recognised as an efficient sorbent for removal of Cr(VI) from water and wastewater solutions [34], this is the first time PPy/Fe_3O_4 nanocomposite has been used as an effective sorbent with enhanced capacity for Cr(VI) removal. Along with PPy/Fe_3O_4 nanocomposite, polypyrrole and iron oxide nanoparticles were also tested for comparison.

2. Experimental procedure

2.1. Materials

Pyrrole (Py) and anhydrous ferric chloride ($FeCl_3$) as oxidant for polymerization of pyrrole were purchased from Sigma–Aldrich (Germany). Py was distilled under reduced pressure prior to use. Potassium dichromate ($K_2Cr_2O_7$) and magnetite (Fe_3O_4) nanoparticles were also obtained from Sigma–Aldrich. Stock solution (1000 mg/L) of Cr(VI) was prepared by dissolving $K_2Cr_2O_7$ in deionised water. All other chemicals used in this study were of analytical grade and were freshly distilled before use.

2.2. Synthesis of the adsorbent

The PPy/Fe_3O_4 magnetic nanocomposite was synthesized via in situ chemical oxidative polymerization technique described elsewhere [35]. In a typical polymerization technique, 0.4 g of Fe_3O_4 was added to 80 mL deionised water in a conical flask and ultrasonicated for 10 min for better dispersion of Fe_3O_4 in water. 6 g of $FeCl_3$ (oxidant) was added into the deionised water containing Fe_3O_4 and was shaken for 30 min. To this mixture, 0.8 mL of pyrrole was syringed. Then the reaction mixture was shaken for 3 h at ambient temperature. Finally, to stop the reaction, acetone was added into the reaction mixture. The black powder (nanocomposite) obtained was filtered and washed with distilled water until the filtrate became colourless and thereafter washed with acetone. The nanocomposite was then dried at 100 °C for 6 h under vacuum, until the total mass became constant. By gravimetric analysis, the total weight of the nanocomposite was 1.2 g. The PPy loading in the nanocomposite was 67%.

2.3. Batch experimental systems

2.3.1. Adsorption equilibrium and kinetic experiments

To perform adsorption experiments, Cr(VI) solutions of appropriate concentrations were prepared by diluting the stock solution (1000 mg/L). For equilibrium experiments, the adsorbent mass was fixed at 0.1 g unless otherwise stated. The experiments were carried out by contacting PPy/Fe_3O_4 adsorbent with 50 mL of Cr(VI) samples in 100 mL plastic bottles placed in a thermostatic shaker agitated at 200 rpm for 24 h. The effects of pH, adsorbent dose and temperature on Cr(VI) adsorption capacity were explored. The effect of pH on Cr(VI) adsorption by the PPy/Fe_3O_4 nanocomposite was studied by varying the solution pH from 2.0 to 11.0. The pH of the Cr(VI) solution was adjusted using 0.1 M HCl or 0.1 M NaOH. PPy homopolymer and Fe_3O_4 adsorbents were also tested for comparison under the same experimental condition. The Cr(VI) percentage removal (adsorption efficiency) was determined using Eq. (1):

$$\%\,\text{removal} = \frac{C_0 - C_e}{C_0} \times 100 \tag{1}$$

where C_0 and C_e are the initial Cr(VI) concentration and the equilibrium Cr(VI) concentration, respectively, in mg/L. The effect of PPy/Fe_3O_4 nanocomposite dosage on adsorption of Cr(VI) was examined by varying the mass of adsorbent from 0.025 to 0.25 g. The Cr(VI) initial concentration was 200 mg/L and pH 2.0. The sample volume was 50 mL. The adsorption procedure was similar to that of the effect of pH.

Adsorption isotherm data were generated by performing experiments at 25 °C, 35 °C and 45 °C. At a given temperature and pH 2.0, the initial Cr(VI) concentration was varied from 200 to 600 mg/L. The procedure was similar to that described for the effect of pH. The equilibrium sorption capacity was determined using Eq. (2):

$$q_e = \frac{C_0 - C_e}{m} V \tag{2}$$

where q_e is the equilibrium amount of Cr(VI) adsorbed per unit mass of adsorbent (mg/g) and V is the sample volume (L). From equilibrium uptake information, thermodynamic parameters such as ΔH°, ΔS°, ΔG° were determined.

Adsorption kinetic experiments were carried out by contacting 1.0 g of adsorbent with 1000 mL of Cr(VI) solutions stirred at 300 rpm and operated at 25 °C. The initial Cr(VI) concentration was varied from 50 to 150 mg/L. At time zero and at selected time interval thereafter, 5 mL samples were withdrawn and filtered through a 0.2 μm cellulose acetate filter. The filtrate was analysed for residual amount of Cr(VI) concentration using a spectro-photometer (Photolab-6100). The amount of Cr(VI) adsorbed was calculated using Eq. (3):

$$q_t = \frac{C_0 - C_t}{m} V \tag{3}$$

where q_t is the time-dependent amount of Cr(VI) adsorbed per unit mass of adsorbent (mg/g), C_t is the bulk-phase Cr(VI) concentration (mg/L) at any time t and m is the adsorbent mass (g).

2.3.2. Desorption experiment

To test the regenerability and reusability of the adsorbent, desorption experiments were conducted in a batch mode. At first 100 mg/g of Cr(VI) was loaded onto PPy/Fe_3O_4 nanocomposite by contacting 0.1 g adsorbent with 200 mg/L of Cr(VI) solution (50 mL) at pH 2.0. Then for desorption, the Cr(VI) loaded adsorbent was contacted with 50 mL of NaOH solutions in a thermostatic shaker for 24 h. The concentration range of NaOH was from 0.1 to 1.0 M. At the end of the experiment, Cr(VI) in the solution was measured. The amount of Cr(VI) desorbed was determined by performing appropriate mass balance. To regenerate the spent adsorbent for the next adsorption–desorption cycles, the adsorbent was treated with 2 M HCl. Three consecutive adsorption–desorption cycles, using the same adsorbent were examined to test the reusability of the adsorbent.

2.4. Characterization of PPy/Fe_3O_4 nanocomposite

The structure of the PPy/Fe_3O_4 nanocomposite was characterized by attenuated total reflectance (ATR) Fourier transform infrared (FTIR) spectroscopy. ATR-FTIR spectra were performed on a Perkin-Elmer Spectrum 100 spectrometer, equipped with an FTIR microscopy accessory and a germanium crystal. The field-emission scanning electron microscopy (FE-SEM) and high-resolution transmission electron microscopy (HR-TEM) were used to characterize the morphology of the nanocomposites. FE-SEM images with energy dispersive X-ray analysis (EDX) were obtained on a LEO, Zeiss SEM. TEM specimen was prepared by putting a drop of dilute suspensions of the samples in 2-propanol on copper grid. Elemental composition and chemical oxidation state of the surface species and near surface species of the nanocomposite were determined using X-ray photoelectron spectroscopy (XPS) on a Kratos Axis Ultra device, with an Al monochromatic X-ray source (1486.6 eV). Survey spectra were acquired at 160 eV and region spectra at 20 eV pass energies, respectively. X-ray diffraction patterns were measured on a PANalytical X'Pert PRO-diffractometer using Cu Kα radiation (wavelength, λ = 1.5406 Å) with variable slits at 45 kV/40 mA. Magnetic property of the nanocomposites was confirmed by JEOL-Electron Spin Resonance (ESR) spectrometer.

3. Results and discussion

3.1. Characterization of the PPy/Fe_3O_4 nanocomposite before and after Cr(VI) adsorption

To confirm the presence of PPy and adsorption of Cr(VI) onto the PPy/Fe_3O_4 nanocomposites, ATR-FTIR analyses were done and are shown in Fig. 1. The FTIR spectrum of the PPy/Fe_3O_4 nanocomposite before adsorption (Fig. 1a) demonstrated peaks at 1513, 1423, 1080 and 958–826 cm^{-1} that are considered to arise from pyrrole ring stretching, conjugated C–N stretching, C–H stretching vibration and C–H deformation, respectively, for PPy homopolymer [36,37]. These results confirmed the presence of PPy moieties in the nanocomposite. Interestingly, all peak positions shifted towards higher values after Cr(VI) ions adsorption (Fig. 1b). The delocalized π electrons in PPy matrix, which are involved in the skeletal vibration of PPy ring, are affected by the doping ions in the polymer matrix [35,38]. Different types of dopants in the PPy backbone may disturb the conjugate structure of PPy and this limited the extent of charge delocalization along the polymer chains, leading to red shift [32]. The new two peaks at 774 and 901 cm^{-1} (Fig. 1b) are intrinsic vibration of the Cr–O and Cr=O bonds, respectively [39]. This feature indicates that Cr(VI) ions adsorbed on the surface of the PPy/Fe_3O_4 nanocomposite by replacing doping Cl^- ions.

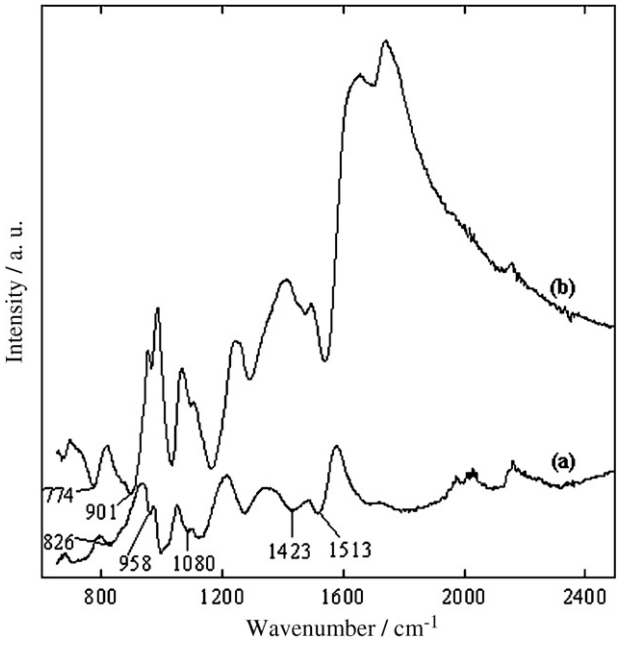

Fig. 1. ATR-FTIR spectra of (a and b) PPy/Fe_3O_4 nanocomposite before and after Cr(VI) adsorption.

The morphologies of Fe_3O_4 and PPy/Fe_3O_4 nanocomposite before and after Cr(VI) adsorption were explored and it was found that Fe_3O_4 nanoparticles are nearly spherical but exist in aggregated form (see supporting document 1). After in situ polymerization process, nearly spherical particles with sizes larger than those of Fe_3O_4 nanoparticles originating from the encapsulation of the Fe_3O_4 nanoparticles by the precipitating PPy moieties in aqueous medium are observed. The surface morphology of the nanocomposite after adsorption with Cr(VI) did not change (see supporting document 1).

Energy dispersive X-rays (EDX) was used to analyse the elemental constituents of the PPy/Fe_3O_4 nanocomposite before and after Cr(VI) adsorption. Fig. 2a (nanocomposite before adsorption) shows

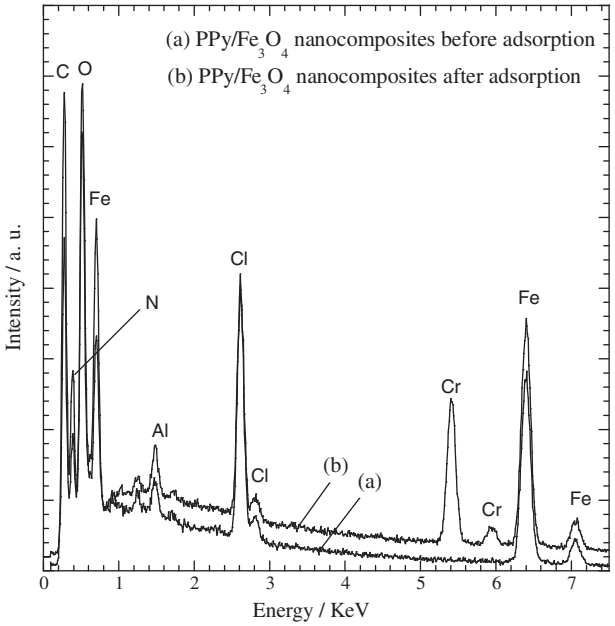

Fig. 2. EDX spectra of (a and b) PPy/Fe_3O_4 nanocomposite before and after Cr(VI) adsorption.

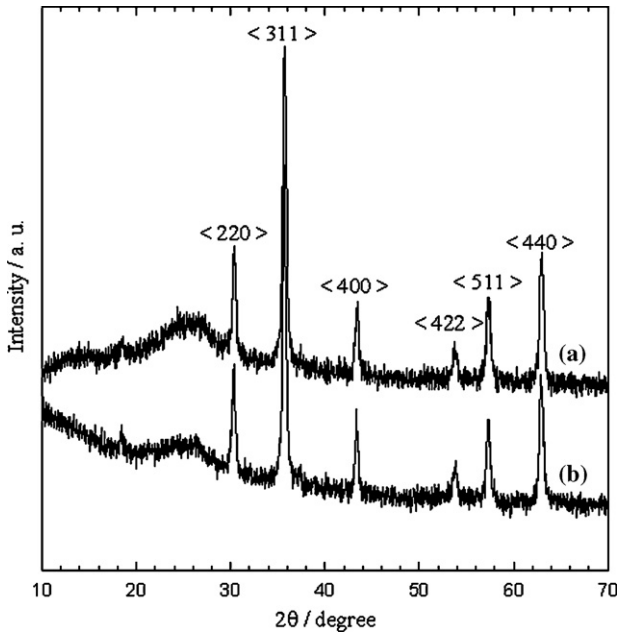

Fig. 3. XRD pattern of (a and b) PPy/Fe_3O_4 nanocomposite before and after Cr(VI) adsorption.

C peak at 0.24 keV, O peak at 0.52 keV, N peak at 0.4 keV, Cl peak at 2.61 keV, and Fe peaks at 0.69 and 6.41 keV. Upon Cr(VI) adsorption, additional peaks of Cr at 5.4 and 5.9 keV are observed (Fig. 2b) [40]. Thus EDX analyses provide a direct evidence for Cr(VI) adsorption on the surface of the nanocomposite.

The TEM images of Fe_3O_4 and PPy/Fe_3O_4 nanocomposite before adsorption confirmed that the prepared media were indeed nanoscale in size and moreover, Fe_3O_4 was encapsulated into the PPy matrix, forming a core–shell structure (see supporting document 2).

The crystalline structure of the adsorbent before and after adsorption of Cr(VI) ions was characterized by XRD as shown in Fig. 3. The diffraction peaks at 30.22° (2 2 0), 35.66° (3 1 1), 43.25° (4 0 0), 53.55° (4 2 2), 57.25° (5 1 1) and 62.88° (4 4 0) are associated with Fe_3O_4 [41]. The observed peaks of Fe_3O_4 are consistent with the database in JCPDS file (PCPDFWIN v.2.02, PDF NO. 85-1436) and also reveal that the core of the nanocomposites is pure Fe_3O_4 phase with a spinal structure. A broad peak is observed at $2\theta = 25.66°$, which is attributed to PPy suggesting some degree of crystallinity in the PPy [42]. Thus XRD results indicate that there is no visual change in the crystalline structure of the nanocomposite after Cr(VI) adsorption.

The magnetic property of the PPy/Fe_3O_4 nanocomposite before and after Cr(VI) adsorption was explored using ESR spectroscopy. The ESR spectra are shown in Fig. 4. From Fig. 4A it can be seen that the line shapes are symmetrical and also the peak to peak line width is very large (~140 mT). This large line width is characteristic of magnetic particles and is due to magnetic inhomogeneity [35,43,44]. Further the line shape does not fit to a 100% Lorentzian or Gaussian function. Instead the best fitting of the line shape occurs with a mixture of 90% Gaussian and 10% Lorentzian functions. It is to be noted that a dominant Gaussian fit is characteristic of ferromagnetic resonance [43] indicating that the predominant fraction of the PPy/Fe_3O_4 nanocomposite is magnetic. Fig. 4B shows that the signal line shapes and widths of the PPy/Fe_3O_4 nanocomposite do not change considerably for after Cr(VI) adsorption, indicating that the magnetic state of the PPy/Fe_3O_4 nanocomposite remains the same. Similar results were obtained in water defluoridation using PPy/Fe_3O_4 nanocomposite [35]. The magnetic property of

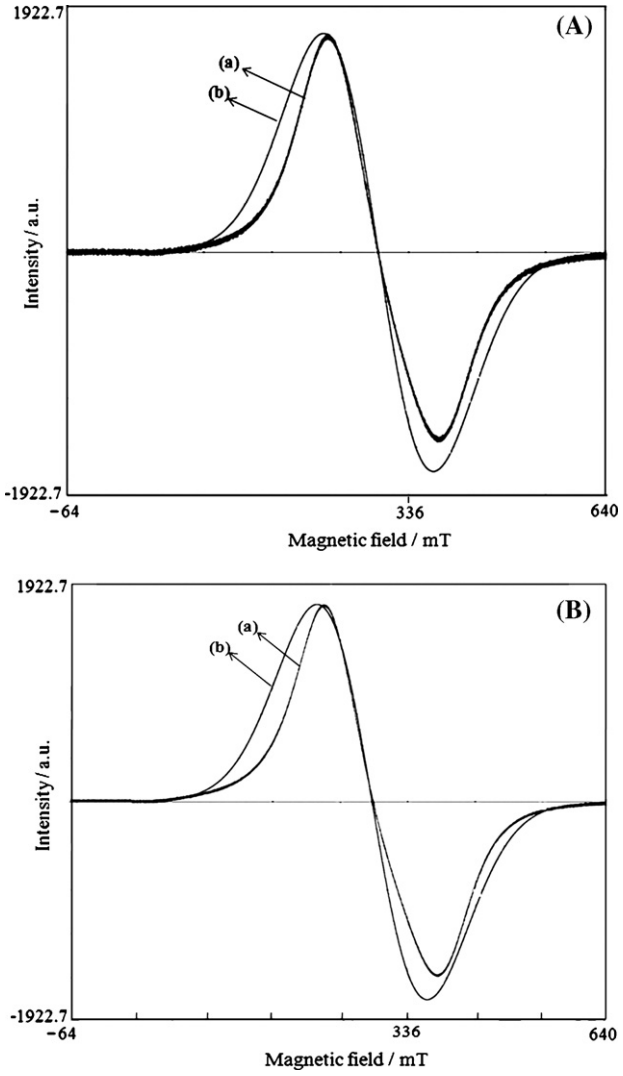

Fig. 4. ESR spectra of (A) (a) PPy/Fe3O4 before adsorption with Cr (VI), (b) 90% Gaussian fitting and 10% Lorentzian and (B) (a) PPy/Fe_3O_4 after adsorption with Cr (VI), (b) 90% Gaussian fitting and 10% Lorentzian.

the nanocomposite was also corroborated as shown in Scheme 1 in which the nanocomposite particles after Cr(VI) adsorption are attracted by magnetic bar. This provides a good prospect for cost effective application of the nanocomposite in magnetic adsorption for industrial wastewater treatment.

3.2. *Effect of pH*

The effect of initial solution pH on Cr(VI) percentage removal by the PPy/Fe_3O_4 nanocomposite and its constituents (PPy and Fe_3O_4) is shown in Fig. 5a. It is evident that the highest (100%) Cr(VI) removal efficiency was found for the PPy/Fe_3O_4 nanocomposite, whereas for polypyrrole (PPy) and iron oxide (Fe_3O_4), removal efficiencies recorded were 73.5% and 40.5%, respectively, at pH 2.0. Therefore, the PPy/Fe_3O_4 nanocomposite can be considered as a highly efficient adsorbent for the removal of Cr(VI) compared to its components PPy and Fe_3O_4. With the increase in pH, Cr(VI) ions removal by the nanocomposite decreases from 100% (at pH 2.0) to 57% (at pH 11.0). It reported that the speciation of Cr(VI) in aqueous solution is strongly pH-dependent. In the range of pH 2.0–6.0, the predominant Cr(VI) species are monovalent bichromate ($HCrO_4^-$) and divalent dichromate ($Cr_2O_7^{2-}$) and above pH 6, the dominant species is chromate (CrO_4^{2-}) ions [7]. The higher

removal efficiency in the acidic pH (2–6) range is due to the anion exchange property of the PPy/Fe_3O_4 nanocomposite by replacing the doped Cl^- ions with either $HCrO_4^-$ or $Cr_2O_7^{2-}$ ions. A plausible mechanism for the removal of $HCrO_4^-$ is shown in Scheme 2. Reduction of Cr(VI) removal efficiency under the alkaline pH is due to the competitive interaction between the hydroxyl (OH^-) ions and CrO_4^{2-} ions for the same sorption sites on the adsorbent surface.

3.3. Effect of adsorbent dose

The effect of the PPy/Fe_3O_4 nanocomposite dose on Cr(VI) removal from aqueous solution is shown in Fig. 5b. It is shown that Cr(VI) percentage removal increases with an increase in PPy/Fe_3O_4 dose. Specifically, the extent of Cr(VI) removal from 50 mL of 200 mg/L Cr(VI) solution, changes from 16.3% at a dose of 0.025 g to 100% at a dose 0.10 g (equivalent of 2 g/L) of PPy/Fe_3O_4. The increase in the amount of the PPy/Fe_3O_4 nanocomposite is significantly influenced the extent of adsorption due to the increase in the number of active sites available for adsorption. In similar studies to explore the effect of adsorbent dose on Cr(VI) removal, Zhang et al. using polyaniline doped with sulfuric acid found that 4 g/L was required to achieve 100% removal of Cr(VI) from aqueous solution containing 50 mg/L [45]. Ansari and Fahim [34] used up to 24 g/L of polypyrrole coated on wood sawdust to achieve 100% removal of Cr(VI) from a solution initially containing 100 mg/L while to effect a 100% removal of Cr(VI) from a solution containing only 3 mg/L, Hu et al. [46] found that 1.4 g/L of oxidized multiwalled carbon nanotubes was required. From those observations, it can be concluded that PPy/Fe_3O_4 nanocomposite is a more effective adsorption media for the removal of Cr(VI) from aqueous solution.

3.4. Adsorption isotherm

In order to describe the interaction between an adsorbate and an adsorbent and to design and operate an adsorption system successfully, equilibrium adsorption isotherm data is important. The adsorption isotherms of Cr(VI) removal by PPy/Fe_3O_4 nanocomposite at temperatures of 25 °C, 35 °C and 45 °C are shown in Fig. 5c. It is observed that there is an increase in the uptake of Cr(VI) with an increase in temperature. This may be due to an increase in thermal energy of the adsorbing species which leads to higher adsorption capacity. This indicates that Cr(VI) adsorption by the PPy/Fe_3O_4 nanocomposite is endothermic in nature. Two extensively used isotherm model viz. Langmuir and Freundlich models were employed to investigate the isotherm data. The linearized Langmuir isotherm model is represented by Eq. (4):

$$\frac{C_e}{q_e} = \frac{1}{q_m b} + \frac{C_e}{q_m} \tag{4}$$

where q_m (mg/g) is the maximum adsorption capacity and b (L/mg) is the Langmuir constant related to the energy of adsorption. Further, the dimensionless separation factor, R_L, which is an essential characteristic of the Langmuir model for defining the favourability of an adsorption process was used. The R_L is given by

$$R_L = \frac{1}{1 + bC_0} \tag{5}$$

Meanwhile the linear form of Freundlich model is expressed as:

$$\ln q_e = \ln K_F + \frac{1}{n} \ln C_e \tag{6}$$

where K_F and $1/n$ constants are related to the adsorption capacity and intensity of adsorption, respectively.

Fig. 6a and b represents the linearized Langmuir and Freundlich isotherm plots for the three different temperatures studied. The Langmuir and Freundlich isotherm parameters calculated from the slope and intercept of the linear equations are given in Table 1. The higher values of correlation coefficient reveal that Langmuir model fitted well the isotherm data compared to the Freundlich model. The maximum adsorption capacity increases from 169.5 to 243.9 mg/g as the temperature is increased from 25 °C to 45 °C. The values of R_L at different temperatures are found to be in the range 0–1 indicating that the adsorption process is favourable.

Table 2 summarizes the Langmuir maximum adsorption capacity and equilibrium time for the removal of Cr(VI) by various adsorbents reported in the literature. It is found that the adsorption capacity of the PPy/Fe_3O_4 nanocomposite is significantly higher than the capacity of other adsorbents. Moreover, the equilibrium time for the removal of Cr(VI) by the PPy/Fe_3O_4 nanocomposite is quite competitive. These results suggest that the PPy/Fe_3O_4 nanocomposite can be considered as a promising adsorbent for the removal of Cr(VI) from industrial wastewater.

3.5. Thermodynamic study

The thermodynamic parameters such as changes in entropy (ΔS°), enthalpy (ΔH°) and standard Gibbs free energy (ΔG°) for the adsorption of Cr(VI) (at initial concentration of 600 mg/L) by the PPy/Fe_3O_4 were determined by using the following equations:

$$\ln\left(\frac{mq_e}{C_e}\right) = \frac{\Delta S^\circ}{R} + \frac{-\Delta H^\circ}{RT} \tag{7}$$

$$\Delta G^\circ = -RT \ln\left(\frac{mq_e}{C_e}\right) \tag{8}$$

where m is the adsorbent dose (g/L), R (J/mol/K) is the gas constant and T is the temperature in K. The ratio mq_e/C_e is referred to as adsorption affinity. A plot of $\ln(mq_e/C_e)$ versus $1/T$ according to Eq. (7) is shown in Fig. 6c. From the plot, both the change in

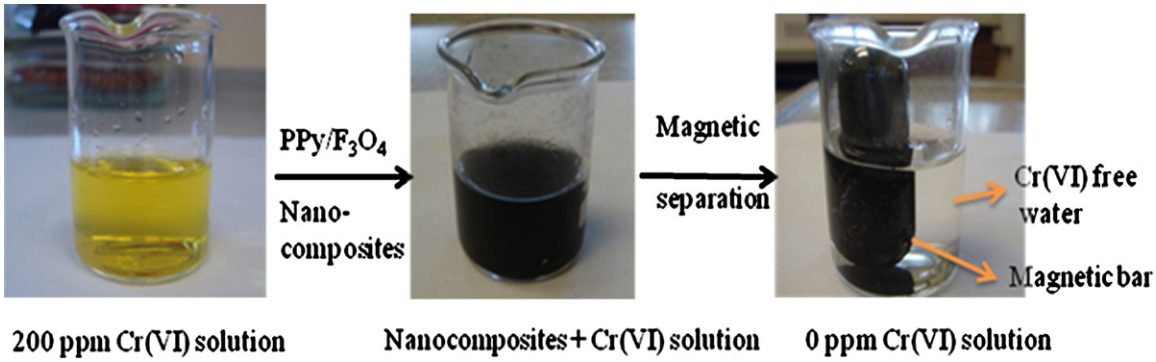

Scheme 1. A photographic representation of Cr(VI) removal from aqueous solution and magnetic separation of used PPy/Fe_3O_4 nanocomposite.

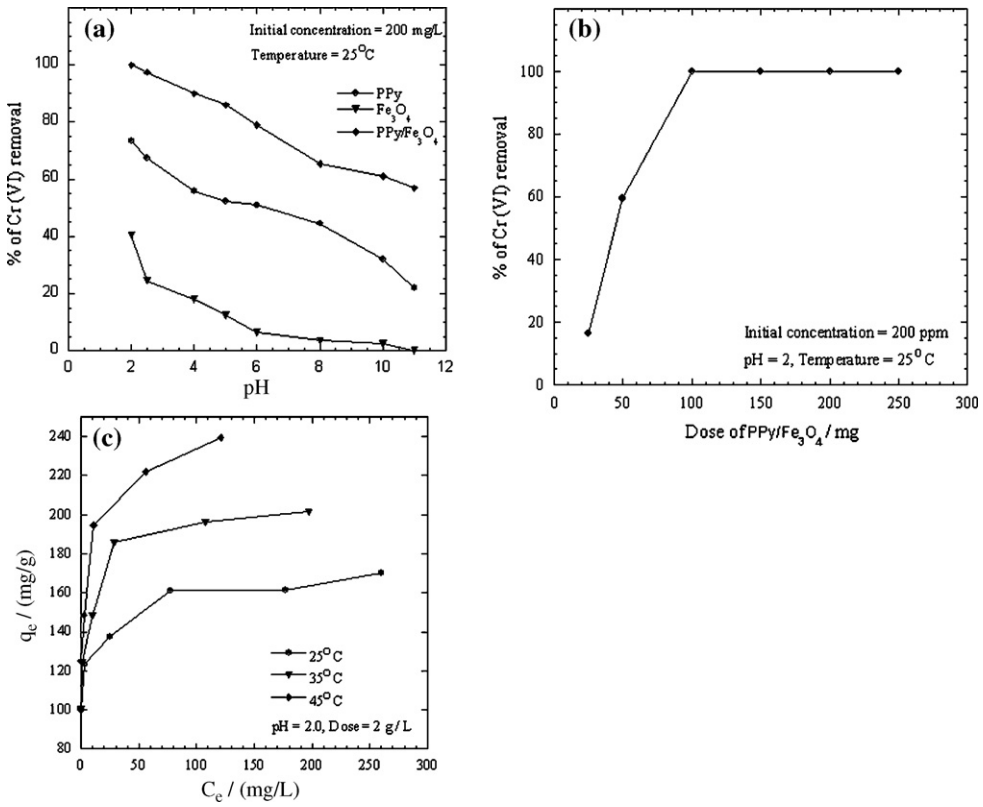

Fig. 5. (a) Effect of pH on the removal of Cr(VI) by the PPy/Fe_3O_4 nanocomposite, PPy and Fe_3O_4 nanoparticles. (b) Effect of adsorbent dosage on the removal of Cr(VI) by PPy/Fe_3O_4 nanocomposite. (c) Adsorption isotherms of Cr(VI) onto PPy/Fe_3O_4 nanocomposite.

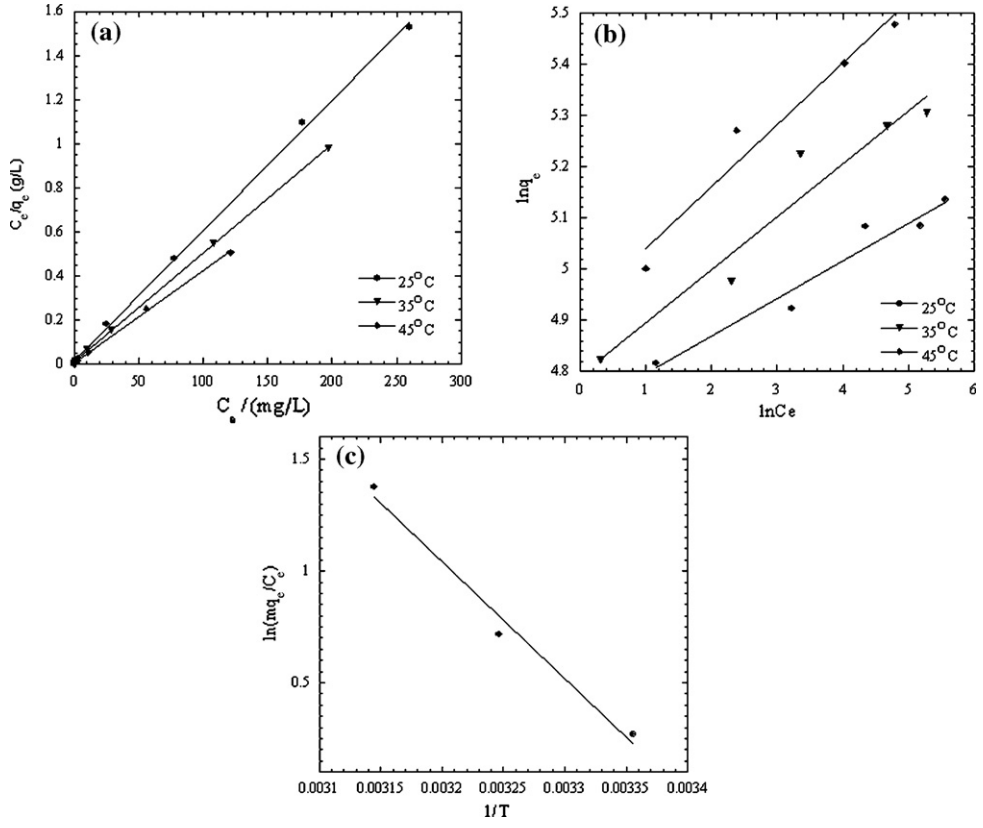

Fig. 6. (a) Fit of equilibrium data to Langmuir isotherm model. (b) Fit of equilibrium data to Freundlich isotherm model. (c) Plot to determine thermodynamic parameters of Cr(VI) adsorption onto PPy/Fe_3O_4 nanocomposite.

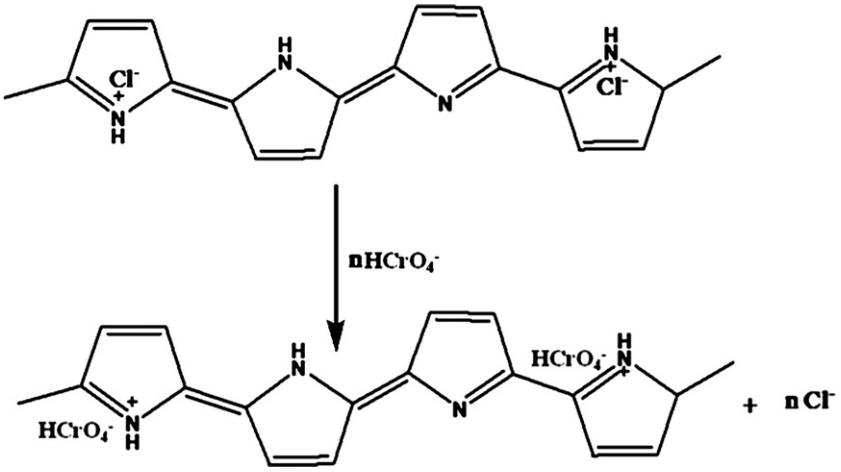

Scheme 2. A plausible mechanism for the removal of Cr(VI) ions from aqueous solution.

Table 1
Langmuir and Freundlich isotherm parameters for Cr(VI) adsorption onto PPy/Fe_3O_4 nanocomposite.

Temperature (°C)	Langmuir constants				Freundlich constants		
	q_m (mg/g)	b (L/mg)	R_L	R^2	K_F (mg/g)	$1/n$	R^2
25	169.49	0.33	0.014	0.998	112.17	0.074	0.952
35	204.08	0.50	0.009	0.999	121.52	0.103	0.937
45	238.09	0.71	0.006	0.998	137.13	0.120	0.955

Table 2
Comparison of adsorption capacity of the PPy/Fe_3O_4 nanocomposite with other adsorbents for Cr(VI) removal at 25 °C.

Adsorbents	q_m (mg/g)	Equilibrium time (h)	Optimum pH	Ref.
Activated carbon	15.47	3	4.0	[12]
Activated carbon coated with quarternized poly(4-vinylpyridine)	53.7	24	2.25	[47]
Amorphous aluminium oxide	78			[15]
Diatomite-supported magnetite nanoparticles	69.16	1	2.0	[27]
Hydrous zirconium oxide	61	1	2.0	[19]
Surface modified jacobsite	31.55	0.08	2.0	[28]
Oxidized multiwalled carbon nanotubes	2.60	280	2.88	[46]
Bio-functional magnetic beads	5.79	12	1.0	[13]
Nanocrystalline akaganeite	79.66	1.0	5.5	[48]
Polyaniline–polyethylene glycol composite	68.97	0.50	5.0	[49]
Polypyrrole/wood sawdust	3.4	0.16	5.0	[34]
Polypyrrole/F_3O_4 magnetic nanocomposite	169.4–243.9	0.50–3	2.0	[Present study]

entropy (ΔS°) and the enthalpy (ΔH°) of adsorption were determined and are 147.73 J/mol/K and 43.4 kJ/mol, respectively. The positive value of ΔH° is consistent with the endothermic nature of the sorption process while the positive value of ΔS° suggests an increase in disorder at the solid–liquid interface. From Eq. (8) the values of change in standard Gibbs energy was computed and found to be −0.565 kJ/mol, −2.04 kJ/mol and −3.51 kJ/mol at 25 °C, 35 °C and 45 °C, respectively. The decrease in ΔG° values with an increase in temperature indicates the spontaneous nature of the adsorption process.

3.6. Sorption kinetics

In addition to high adsorption capacity, it is essential that an adsorbent offers rapid sorption kinetics for efficient adsorbate removal from solution. Fig. 7 represents the effect of contact time and initial concentration on the removal of Cr(VI). It is observed that Cr(VI) uptake is rapid, and increases with an increase in contact time and with an increase in initial concentration. Furthermore, it required 30–180 min for equilibrium to be reached.

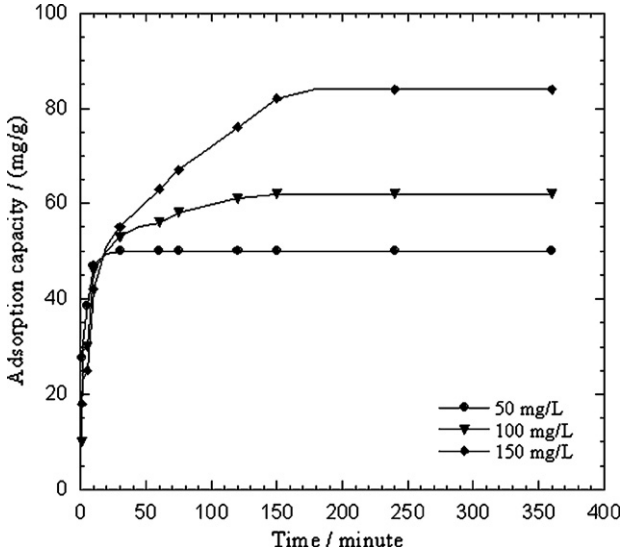

Fig. 7. The effect of initial concentration on the kinetics of Cr(VI) adsorption onto PPy/Fe_3O_4 nanocomposite. Temp = 25 °C and initial solution = pH 2.

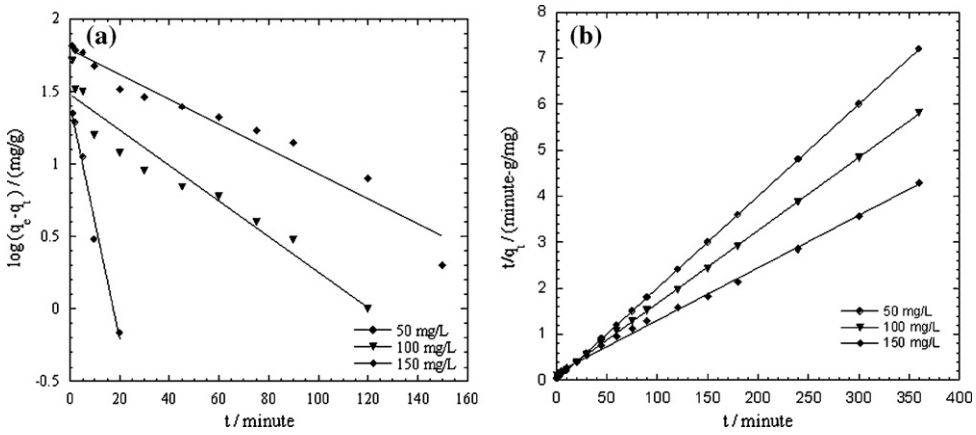

Fig. 8. Pseudo-first-order kinetic model for adsorption of Cr(VI) by the PPY/Fe_3O_4 nanocomposite. (b) Pseudo-second-order kinetic model for adsorption of Cr(VI) by the PPY/Fe_3O_4 nanocomposite.

To understand the kinetic mechanism of the present adsorption process, pseudo-first-order and pseudo-second-order models were used to fit the kinetic data. The linearized forms of the pseudo-first-order and pseudo-second-order equations are given in Eqs. (9) and (10), respectively:

$$\log(q_e - q_t) = \log q_e - \frac{k_1}{2.303}t \quad (9)$$

$$\frac{t}{q_t} = \frac{1}{k_2 q_e^2} + \frac{1}{q_e}t \quad (10)$$

where q_t is Cr(VI) uptake at time t, and k_1 and k_2 are the pseudo first order and second order rate constants, respectively. From pseudo second kinetic model, the initial sorption rate, h_0 (mg/g/min) can be defined as:

$$h_0 = k_2 q_e^2 \quad (t \to 0) \quad (11)$$

The linearized plots of Eqs. (9) and (10) are shown in Fig. 8a and b, respectively. From the plots, the rate constants were determined and together with the correlation coefficients are given in Table 3. From the values of the correlation coefficients, the pseudo-second-order model ($R^2 \approx 0.996$–1.00) gave better description of the Cr(VI) adsorption compared to pseudo-first-order model ($R^2 \approx 0.935$–0.987). Results indicate that pseudo-second-order rate constant (k_2) decreases from 0.037 to 0.0007 g/mg/min for an increase in initial concentration from 50 to 150 mg/L. The initial sorption rate (h_0) varied from 94.4 to 5.86 mg/g/min with a change in initial Cr(VI) concentration from 50 mg/L to 150 mg/L. The calculated values of q_e from the pseudo-second-order model are nearly equal to the experimentally obtained values further suggesting that Cr(VI) adsorption kinetics is described by the pseudo-second-order mechanism.

3.7. Desorption

The regeneration ability of the spent adsorbent material is an important factor to evaluate the cost effectiveness of a media. Desorption of Cr(VI) from the media was performed at different concentrations (0.1–1.0 M) of NaOH solution. In the first cycle only 14% of the adsorbed Cr(VI) could be extracted using 0.5 M NaOH while upon treatment with 2 M HCl, the remaining amount of Cr(VI) which were reduced to Cr(III) (as evident from the total Cr concentration measurement by ICP-OES and XPS analysis) by the electron rich polypyrrole moieties were released and simultaneously the sorption sites were regenerated by the doping Cl^- ions. As shown in the first two cycles in Fig. 9, the adsorption capacity of the nanocomposite was 100 mg/g. In the third cycle the adsorption capacity of the nanocomposite was slightly reduced to 83.1 mg/g. Therefore, the nanocomposite can be successfully reused for two adsorption–desorption cycles without loss of its original adsorption capacity.

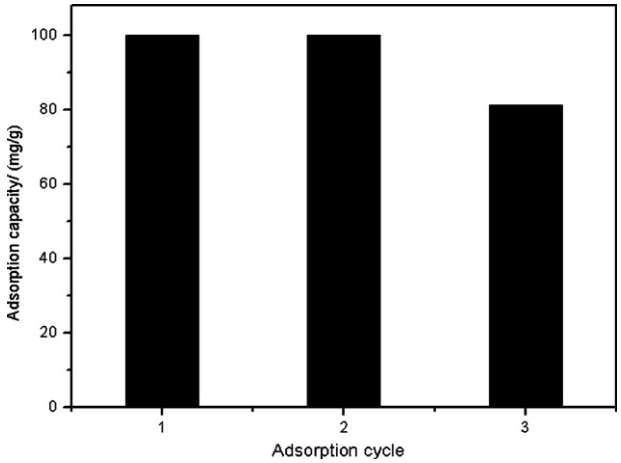

Fig. 9. Adsorption–desorption cycles.

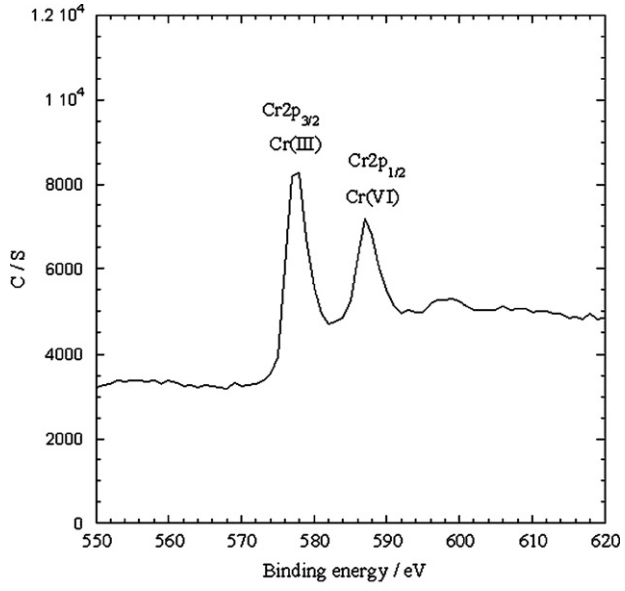

Fig. 10. XPS spectra of the PPy/Fe_3O_4 nanocomposite after Cr(VI) adsorption.

Table 3
Kinetic parameters for Cr(VI) adsorption onto PPy/Fe_3O_4 nanocomposite.

C_0 (mg/L)	Pseudo-first-order model			Pseudo-second-order model		
	K_1 (1/min)	q_e (mg/g)	R^2	K_2 (g/mg/min)	q_e (mg/g)	R^2
50	0.188	4.15	0.987	0.037	50.00	1.00
100	0.028	4.39	0.935	0.003	63.29	0.999
150	0.019	6.03	0.950	0.0007	87.71	0.996

3.8. Adsorption mechanism

To investigate the mechanism of adsorption, Cr(VI) loaded PPy/Fe_3O_4 nanocomposite was subjected to X-ray photoelectron spectroscopy (XPS). Fig. 10 shows the XPS spectra of the nanocomposite after Cr(VI) adsorption at pH 2.0. Two energy bands at about 577.5 eV and 587.2 eV corresponding to the binding energies of Cr ($2p_{3/2}$) and Cr ($2p_{1/2}$) orbital's, respectively, are observed [7,43]. This observation suggests the existence of both Cr(III) and Cr(VI) on the adsorbent surface. The existence of Cr(VI) species on the surface of the adsorbent is consistent with the sorption of Cr(VI) ions due to the anion exchange property of PPy by replacing the doped Cl^- ions as shown in Scheme 2. The presence of Cr(III) on the nanocomposite surface suggests that some fraction of adsorbed Cr(VI) was reduced to Cr(III) by a reduction process. The reduction process may be due to the presence of electron rich polypyrrole moieties in the nanocomposite [36,37].

4. Conclusions

Magnetic nanocomposites are emerging materials for the removal of contaminants from water. In the present work, PPy/Fe_3O_4 nanocomposite was synthesized, characterized and used as an effective sorbent for the removal of Cr(VI) form aqueous solution. The results indicated that removal efficiency is highly pH dependent and 100% removal was obtained at pH 2.0 when the initial Cr(VI) concentration was 200 mg/L. Chromium adsorption was rapid and it required 30–180 min for equilibrium to be reached. Langmuir isotherm model was found to describe the equilibrium isotherm data. The kinetic data fitted to the pseudo-second order model. Thermodynamic parameters confirmed the spontaneous and endothermic nature of the adsorption process. Desorption studies revealed that only 14% of the sorbed Cr(VI) could be desorbed with 0.5 M NaOH. Upon using 2 M HCl, the PPy/Fe_3O_4 nanocomposite could be reused for two consecutive adsorption–desorption cycles without appreciable loss of its original capacity. From XPS analysis, ion exchange and reduction has been detected as the leading mechanism of Cr(VI) adsorption. This work involved the use of single-ion solution. Real wastewater contains a number of contaminants that may affect the performance of the material. Thus, further studies are required to asses the potential of the media in the removal of Cr(VI) from industrial wastewater.

Acknowledgement

The authors wish to express their sincere gratitude to the National Research Foundation (NRF) of South Africa for the financial support under Nanotechnology Flagship Grant.

Appendix A. Supplementary data

Supplementary data associated with this article can be found, in the online version, at doi:10.1016/j.jhazmat.2011.03.062.

References

[1] M.K. Aroua, F.M. Zuki, N.M. Sulaiman, Removal of chromium ions from aqueous solutions by polymer-enhanced ultrafiltration, J. Hazard. Mater. 147 (2007) 752–758.
[2] T.N. De castro Dentas, A.A. Dantas Neto, A. De, M.C.P. Moura, E.L. Barros Neto, E. de paiva Telemaco, Chromium adsorption by chitosan impregnated with microemulsion, Langmuir 17 (2001) 4256–4260.
[3] S.A. Katz, H. Salem, The toxicology of chromium with respect to its chemical speciation: a review, J. Appl. Toxicol. 13 (1993) 217–224.
[4] A.M. Yusof, N.A.N.N. Malek, Removal of Cr(VI) and As(V) from aqueous solutions by HDTMA-modified zeolite, J. Hazard. Mater. 162 (2009) 1019–1024.
[5] EPA (Environmental Protection Agency), Environmental Pollution Control Alternatives, EPA/625/5-90/025, EPA/625/4-89/023, Cincinnati, US, 1990.
[6] J.W. Patterson, Industrial Wastewater Treatment Technology, 2nd ed., Butterworth-Heinemann, London, 1985.
[7] J. Hu, G.H. Chen, I.M.C. Lo, Removal and recovery of Cr(VI) from wastewater by maghemite nanoparticles, Water Res. 39 (2005) 4528–4536.
[8] N.R. Bishnoi, M. Bajaj, N. Sharma, A. Gupta, Adsorption of Cr(VI) on activated rice husk carbon and activated alumina, Bioresour. Technol. 91 (2004) 305–307.
[9] M. Dakiky, M. Khamis, A. Manassra, M. Mereb, Selective adsorption of Cr(VI) in industrial wastewater using low-cost abundantly available adsorbents, Adv. Environ. Res. 6 (2002) 533–540.
[10] K. Selvi, S. Pattabhi, K. Kadirvelu, Removal of Cr(VI) from aqueous solution by adsorption onto activated carbon, Bioresour. Technol. 80 (2001) 87–89.
[11] D. Mohan, K.P. Sing, V.K. Sing, Removal of hexavalent chromium from aqueous solution using low cost activated carbon derived from agricultural waste materials and activated carbon febric cloth, Ind. Eng. Chem. Res. 44 (2005) 1027–1042.
[12] B. Sandhya, A.K. Tonni, Cr(VI) removal from synthetic wastewater using coconut shell charcoal and commercial activated carbon modified with oxidizing agents and/or chitosan, Chemosphere 54 (2004) 951–967.
[13] H. Li, Z. Li, T. Liu, X. Xiao, Z. Peng, L. Deng, A novel technology for biosorption and recovery hexavalent chromium in wastewater by bio-functional magnetic beads, Bioresour. Technol. 99 (2008) 6271–6279.
[14] R. Chand, K. Narimura, H. Kawakita, K. Ohto, T. Watari, K. Inoue, Grape waste as a biosorbent for removing Cr(VI) from aqueous solution, J. Hazard. Mater. 163 (2009) 245–250.
[15] E. Alvarez-Ayuso, A. Garcia-Sanchez, X. Querol, Adsorption of Cr(VI) from synthetic solutions and electroplating wastewaters on amorphous aluminium oxide, J. Hazard. Mater. 142 (2007) 191–196.
[16] V. Goshu, Y.V. Tsarev, V.V. Kastrov, Kinetics of chromium(VI) adsorption from model solutions on iron oxide, Russ. J. Appl. Chem. 82 (2009) 801–804.
[17] S. Debnath, U.C. Ghosh, Kinetics, isotherm and thermodynamics for Cr(III) and Cr(VI) adsorption from aqueous solutions by crystalline hydrous titanium oxide, J. Chem. Thermodyn. 40 (2008) 67–77.
[18] S. Goswami, U.C. Ghosh, Studies on adsorption behaviour of Cr(VI) onto synthetic hydrous stannic oxide, Water SA 31 (2005) 597–602.
[19] L.A. Rodrigues, L.J. Maschio, R.E. da Silva, M.L.C. Pinto da Silva, Adsorption of Cr(VI) from aqueous solution by hydrous zirconium oxide, J. Hazard. Mater. 173 (2010) 630–636.
[20] D.R. Mulinari, G.L.J.P. Siva, M.L.C.P. Silva, Adsorption of dichromate ions on the cellulose/$ZrO_2 \cdot nH_2O$ prepared by the methods of conventional precipitation and homogeneous solution precipitation, Quim. Nova 29 (2006) 496–500.
[21] N. Savage, M.S. Diallo, Nanomaterials and water purification: opportunities and challenges, J. Nanopart. Res. 7 (2005) 331–342.
[22] X. Zhao, Y. Shi, Y. Cai, S. Mou, Cetyltrimethylammonium bromide coated magnetic nanoparticles for the preconcentration of phenolic compounds from environmental water samples, Environ. Sci. Technol. 42 (2008) 1201–1206.
[23] A.F. Ngomsik, A. Bee, M. draye, G. Cote, V. Cabuil, Magnetic nano- and microparticles for metal removal and environmental applications: a review, Comptes Rendus Chimie 8 (2005) 963–970.
[24] L. Li, M. Fan, R.C. Brown, L.J. HansVan, J. Wang, W. Wang, Y. Song, P. Zhang, Synthesis, properties, and environmental applications of nanoscale iron-based materials: a review, Crit. Rev. Environ. Sci. Technol. 36 (2006) 405–431.
[25] R.C. O'Handley, Modern Magnetic Materials. Principles and Applications, John Wiley and Sons, New York, 2000.
[26] J. Hu, I.M.C. Lo, G. Chen, Removal of Cr(VI) by magnetite nanoparticles, Water Sci. Technol. 50 (2004) 139–146.
[27] Y. Peng, D. Liu, M. Fan, D. Yang, R. Zhu, F. Ge, J. Zhu, H. He, Removal of hexavalent chromium [Cr(VI)] from aqueous solutions by the diatomite-supported/unsupported magnetite nanoparticles, J. Hazard. Mater. 173 (2010) 614–621.

[28] J. Hu, I.M.C. Lo, G. Chen, Fast removal and recovery of Cr(VI) using surface-modified jacobsite($MnFe_2O_4$) nanoparticles, Langmuir 21 (2005) 11173–11179.
[29] T.M. Wu, S.H. Lin, Characterization and electrical properties of polypyrrole/multiwalled carbon nanotube composites synthesized by in-situ chemical oxidative polymerization, J. Polym. Sci. Part B: Polym. Phys. 44 (2006) 1413–1418.
[30] G. Han, J. Yuan, G. Shi, F. Wei, Electrodeposition of polypyrrole/multiwalled carbon nanotube composite films, Thin Solid Films 474 (2005) 64–69.
[31] X. Zhang, R. Bai, Surface electric properties of polypyrrole in aqueous solutions, Langmuir 19 (2003) 10703–10709.
[32] X. Zhang, R. Bai, Y.W. Tong, Selective adsorption behaviors of proteins on PPy-based adsorbents, Sep. Purif. Technol. 52 (2006) 161–169.
[33] B. Saoudi, N. Jammul, M.L. Abel, M.M. Chehimi, G. Dodin, DNA adsorption onto conducting polypyrrole, Synth. Met. 87 (1997) 97–103.
[34] R. Ansari, N.K. Fahim, Application of polypyrrole coated on wood sawdust for removal of Cr(VI) ion from aqueous solutions, React. Funct. Polym. 67 (2007) 367–374.
[35] M. Bhaumik, T.Y. Leswifi, A. Maity, V.V. Srinivasu, M.S. Onyango, Removal of fluoride from aqueous solution by ploypyrrole/Fe_3O_4 magnetic nanocomposite, J. Hazard. Mater. 186 (2011) 150–159.
[36] Y. Yu, C. Ouyang, Y. Gao, Z. Si, W. Chen, Z. Wang, G. Xue, Synthesis and characterization of carbon nanotube/polypyrrole core–shell nanocomposites via in situ inverse microemulsion, J. Polym. Sci. Part A: Polym. Chem. 43 (2005) 6105–6115.
[37] A. Maity, S. Sinha Ray, Highly conductive core–shell nanocomposite of polyNvinylcarbazole–polypyrrole with multiwall carbon nanotubes, Macromol. Rapid Commun. 29 (2008) 1582–1587.
[38] M.R. Karim, C.J. Lee, A.M.S. Chowdhury, N. Nahar, M.S. Lee, Radiolytic synthesis of conducting polypyrrole/carbon nanotube composites, Mater. Lett. 61 (2007) 1688–1692.
[39] S. Deng, R. Bai, Removal of trivalent and hexavalent chromium with aminated polyacrylonitrile fibres: performance and mechanisms, Water Res. 38 (2004) 2424–2432.
[40] C.D. Palmer, Precipitates in a Cr(VI)-contaminated concrete, Environ. Sci. Technol. 34 (2000) 4185–4192.
[41] J. Liu, M. Wan, Composites of polypyrrole with conducting and ferromagnetic behaviours, J. Polym. Sci. Part A: Polym. Chem. 38 (2000) 2734–2739.
[42] K. Cheah, M. Forsyth, V.T. Truong, Ordering and stability of conducting polypyrrole, Synth. Met. 94 (1998) 215–219.
[43] O.A. Kuznetsov, O.N. Sorokina, V.G. Leontiev, O.A. Shlyakhtin, A.L. Kovarski, A.A. Kuznetsov, ESR study of thermal demagnetization processes in ferromagnetic nanoparticles with curie temperatures between 40 and 60 °C, J. Magn. Magn. Mater. 311 (2007) 204–207.
[44] V.V. Srinivasu, S.E. Lofland, S.M. Bhagat, Room temperature colossal microwave magneto impedance in micron size powders of $La_{0.7}Ba_{0.3}MnO_3$ and $La_{0.7}Sr_{0.3}MnO_3$—a novel magnetic tape, J. Appl. Phys. 83 (1998) 2866–2868.
[45] R. Zhang, H. Ma, B. Wang, Removal of chromium(VI) from aqueous solution using polyaniline doped with sulfuric acid, Ind. Eng. Chem. Res. 49 (2010) 9998–10004.
[46] J. Hu, C. Chen, X. Zhu, X. Wang, Removal of chromium from aqueous solution by using oxidized multiwalled carbon nanotubes, J. Hazard. Mater. 162 (2009) 1542–1550.
[47] J. Fang, Z. Gu, D. Gang, C. Liu, E.S. Ilton, B. Deng, Cr(VI) removal from aqueous solution by activated carbon coated with quartinized poly(4-vinylpyridine), Environ. Sci. Technol. 41 (2007) 4748–4753.
[48] N.K. Lazaridis, D.N. Bakoyannakis, E.A. Deliyanni, Chromium(VI) sorptive removal from aqueous solution by nanocrystalline akaganeite, Chemosphere 58 (2005) 65–73.
[49] M.R. Samani, S.M. Borghei, A. Olad, M.J. Chaichi, Removal of chromium from aqueous solution using polyanililine–polyethylene glycol composite, J. Hazard. Mater. 184 (2010) 248–254.